Angewandte Chemie
GDCh
Eine Zeitschrift der Gesellschaft Deutscher Chemiker
www.angewandte.de

Akzeptierter Artikel

Titel: Perylene-fused, Aggregation-free Polycyclic Aromatic Hydrocarbons for Solution-processed Distributed Feedback Lasers

Autoren: Ya Zou, Víctor Bonal, Sergio Moles Quintero, Pedro G. Boj, José M. Villalvilla, José A. Quintana, Guangwu Li, Shaofei Wu, Qing Jiang, Yong Ni, Juan Casado, María A. Díaz-García, and Jishan Wu

Zitierweise: *Angew. Chem. Int. Ed.* 10.1002/anie.202004789

Link zur VoR: https://doi.org/10.1002/anie.202004789

WILEY-VCH

10.1002/ange.202004789

WILEY-VCH

RESEARCH ARTICLE

Perylene-fused, Aggregation-free Polycyclic Aromatic Hydrocarbons for Solution-processed Distributed Feedback Lasers

Ya Zou,[†][a] Víctor Bonal,[†][b] Sergio Moles Quintero,[†][c] Pedro G. Boj,[d] José M. Villalvilla,[b] José A. Quintana,[d] Guangwu Li,[a] Shaofei Wu,[a] Qing Jiang,[a] Yong Ni,[a] Juan Casado,*[c] María A. Díaz-García*[b] and Jishan Wu*[a][e]

Abstract: *Perylene-fused, aggregation-free polycyclic aromatic hydrocarbons with partial zigzag periphery (**ZY-01**, **ZY-02**, and **ZY-03**) were synthesized. X-ray crystallographic analysis reveals that there is no intermolecular π-π stacking in all three molecules, and as a result, they show moderate-to-high photoluminescence quantum yield in both solution and solid state. They also display characteristic absorption and emission spectra of perylene dyes. **ZY-01** and **ZY-02** with a nearly planar π-conjugated skeleton exhibit amplified spontaneous emission (ASE) when dispersed in polystyrene thin films. All solution-processed distributed feedback lasers have been fabricated using **ZY-01** and **ZY-02** as active gain materials, both showing narrow emission linewidth (< 0.4 nm) at wavelengths around 515 and 570 nm, respectively. On the other hand, **ZY-03** did not show ASE and lasing, presumably due to its highly twisted backbone, which facilitates non-radiative internal conversion and intersystem crossing.*

Introduction

Large-size disk-like polycyclic aromatic hydrocarbons (PAHs) have been usually considered as effective charge transporting materials due to the strong intermolecular π-π stacking along the self-assembled columnar superstructures.[1] Aggregation however quenches photoluminescence (PL), which limits their applications in solid-state light-emitting devices. To solve this problem, a general strategy is to attach long branched alkyl or alkylphenyl chains,[2] which is favorable for solubility, but still insufficient to fully suppress PL quenching. The PL quantum yield (PLQY) of PAHs is also determined by their edge structure. The all-armchair edged PAHs such as the hexa-*peri*-hexabenzocoronene (HBC) usually show a PLQY of less than 3% in solution mainly due to symmetry-forbidden electronic transitions.[3] On the other hand, PAHs with two or more zigzag-type peripheries show smaller energy gap, however, could have largely improved PLQY.[4]

Optically-pumped organic lasers have received great attention for many years, mainly because they offer the possibility to tune the emission wavelength within the visible range. In the last two decades, thin-film organic lasers (TFOLs) have emerged as a new generation of devices with clear advantages with respect to other types of organic lasers, such as monolithic-based solid-state dye lasers or commercially available liquid dye lasers.[5] While the latter have large sizes and require very powerful laser sources to operate, TFOLs are compact, inexpensive, mechanical flexible and can be pumped with low-power sources, in some cases even with diode lasers or light emitting diodes. Probably the most successful TFOL so far has been the distributed feedback (DFB) laser, which has been designed and fabricated in the present work, consisting of a waveguide film which includes a relief diffractive grating as laser resonator. Besides the aforementioned advantages of TFOLs, the DFB laser can provide single mode emission (useful for certain applications) and the laser cavity is integrated within the device. DFBs have already demonstrated applicability in areas such as spectroscopy, optical communications and sensing.[5] A variety of active organic materials such as semiconducting polymers prepared as neat films[6] and conventional organic dyes dispersed in an thermoplastic polymer film (used as matrix),[7] have been used as efficient gain media towards optically-pumped TFOLs. Photo-stability however is a drawback for these organic materials, particularly under strong irradiation resulting in short operational lifetime. Hence, for practical applications, it is necessary to develop materials simultaneously achieving systematic color tuning, high photo-stability, and low threshold for stimulated emission. Recently, well-defined PAHs[1] emerged as very good candidates due to their relatively high environmental stability and tunability of their optical properties. Stable amplified spontaneous emission (ASE) was first observed from a PAH, dibenzo[*hi,st*]ovalene (DBOV), with remarkable environmental and operational stability.[8] In despite of this, applications in real laser devices with DBOV have not been realized yet. The current team recently demonstrated the very first solution-processed DBF lasers based on three PAHs with four zigzag edges, which showed excellent ASE performance comparable to state-of-the-art reported organic lasers.[9] These promising results indicate that aggregation-free PAHs with partial zigzag edges could be a new type of promising luminescence materials for optically pumped organic lasers. Therefore, we are interested in further developing new strategy towards large-size aggregation-free PAHs with

[a] Y. Zou, Dr. G. Li, S. Wu, Dr. Q. Jiang, Dr. Y. Ni, Prof. J. Wu
Department of Chemistry, National University of Singapore
3 Science Drive 3, 117543, Singapore
Fax: (+65) 6779 1691
E-mail: chmwuj@nus.edu.sg
[b] V. Bonal, Dr. J. M. Villalvilla, Prof. M. A. Díaz-García
Departamento Física Aplicada and Instituto Universitario de Materiales de Alicante, Universidad de Alicante, Alicante 03080, Spain
Email: maria.diaz@ua.es
[c] S. Moles Quintero, Prof. J. Casado
Department of Physical Chemistry, University of Malaga
Campus de Teations s/n, 229071 Malaga, Spain
E-mail: casado@uma.es
[d] Dr. P. G. Boj, Dr. J. A. Quintana
Departamento Óptica, Farmacología y Anatomía and Instituto Universitario de Materiales de Alicante, Universidad de Alicante, Alicante 03080, Spain
[e] Prof. J. Wu
Joint School of National University of Singapore and Tianjin University, International Campus of Tianjin University, Binhai New City, Fuzhou 350207, China

[†] These authors contributed equally to this work.

Supporting Information for this article is given via a link at the end of the document.

10.1002/ange.202004789

WILEY-VCH

tunable properties, and to exploit their applications in solution-processed photo-pumped organic lasers.

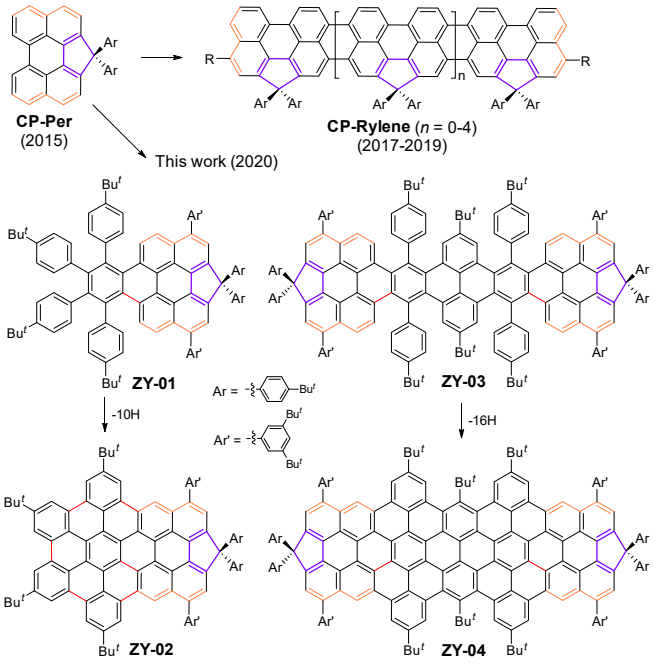

Figure 1. Structures of the cyclopenta-ring fused perylene (CP-Per), rylenes (CP-Rylene), and the targeted perylene-fused aggregation-free PAHs **ZY-01**, **ZY-02**, **ZY-03** and **ZY-04** in this work. The zigzag edges are highlighted in orange colour.

Among various gain materials, perylene and extended perylene (rylenes) are one of the most frequently used dyes in traditional lasers.[6b, 6e] Their molecular structures actually contain two zigzag edges at the *peri*- termini. However, a serious problem is their strong tendency to aggregate. We recently developed a new sp^3-carbon bridged, cyclopenta (CP) ring fused perylene building block (CP-Per),[10] which has been used to synthesize a series of soluble and aggregation-free long rylenes (CP-Rylene) (Figure 1).[11] The attachment of two aryl groups onto the sp^3 carbons in a wedge-like manner thwarts significant intermolecular π–π contacts. In addition, our recent studies showed that regio-selective functionalization could be done at both *peri*- and *bay*-positions,[12] which opened the opportunities to construct large-size aggregation-free PAHs from the CP-ring fused perylene. In this work, we first report our synthetic effort towards a series of CP-Per fused PAHs such as the partially fused **ZY-01**/**ZY-03**, and the fully fused **ZY-02**/**ZY-04**. Their geometry by X-ray crystallography discloses large intermolecular distances preventing aggregation. Their optical properties have been investigated and compared to those of the traditional perylene dyes and other large-size PAHs such as HBC derivatives. Then, their ASE properties were probed in polystyrene (PS) thin films doped with a small amount of chromophores. Finally, all-solution processed lasers with polymeric second-order DFB resonators were fabricated and characterized. The relationship between the molecular structure and ASE/lasing property will be briefly discussed.

Results and Discussion

Synthesis. In addition to the bis-4-*tert*-butylphenyl (Ar) groups at the CP unit, other bulky *tert*-butyl (Bu^t) or 3,5-di-*tert*-butylphenyl (Ar') groups are also attached onto the π-conjugated skeleton to further suppress aggregation and improve solubility (Figure 1). The key building block is compound **7** containing a terminal alkyne unit at the bay region, which allows Diels-Alder cycloaddition and subsequent Scholl-type cyclodehydrogenation reaction (Scheme 1). The synthesis started from 3-formylperylene **1**.[10] Reaction of **1** with 4-ethyl-1-methyl-4H-[1,2,4]triazol-1-ium iodide (EMTI)[13] gave the perylene monoester **2** in nearly quantitative yield. Treatment of **2** with excess of 4-*tert*-butylphenyl lithium generated the alcohol intermediate, and subsequent $BF_3{\cdot}Et_2O$ mediated Friedel−Crafts alkylation provided the CP-ring fused perylene **3** in an overall 90% yield. Bromination of **3** by *N*-bromosuccinimide (NBS) afforded the dibromo- perylene **4** in nearly quantitative yield. Then, the 3,5-di-*tert*-butylphenyl substituted perylene **5** was synthesized in 86% yield by Suzuki coupling reaction from **4**. Formylation of **5** by using CH_3OCHCl_2 and $SnCl_4$ regio-selectively gave the intermediate compound **6** in 55% yield. The aldehyde group in **6** was then converted into ethynylene unit by reaction with dimethyl 1-diazo-2-oxopropyl phosphonate in the presence of base[14] and afforded the key intermediate **7** in 90% yield. Diels-Alder cycloaddition between **7** and 2,3,4,5-tetrakis(4-*tert*-butylphenyl)cyclopenta-2,4-dienone (**8**)[15] or biscyclopentadienone derivative **9**[16] in diphenyl ether (200 °C) provided the oligophenylene substituted precursors **10** and **11** in 78% and 38% yield, respectively. Interestingly, oxidative cyclodehydrogenation of **10** and **11** by using 2,3-dichloro-5,6-

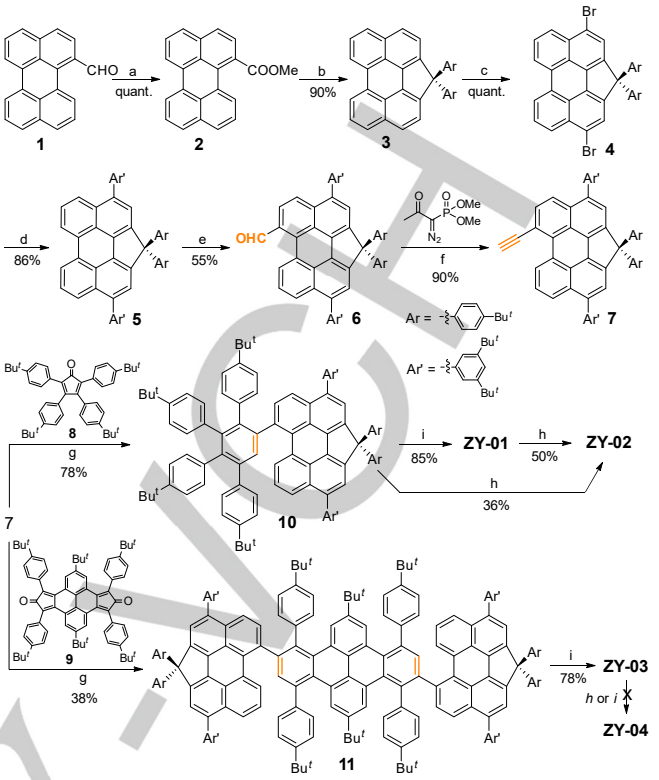

Scheme 1. Synthetic routes of CP-Per fused PAHs: (a) EMTI, DBU,THF, MeOH, rt; (b) i) 4-*tert*-butylbromobenzene, *n*-BuLi, THF, -78 °C; ii) $BF_3{\bullet}Et_2O$, CH_2Cl_2, rt; (c) NBS, $CHCl_3$, rt; (d) 2-(3,5-di-*tert*-butylphenyl)-4,4,5,5-tetramethyl-1,3,2-dioxaborolane, $Pd(PPh_3)_4$, K_2CO_3, toluene/EtOH/H_2O, 100 °C; (e) CH_3OCHCl_2, $SnCl_4$, CH_2Cl_2, reflux; (f) K_2CO_3, MeOH, rt; (g) Ph_2O, 200 °C; (h) $FeCl_3$, CH_2Cl_2, $MeNO_2$, rt; (i) DDQ, $MeSO_3H$, CH_2Cl_2, rt. DBU: 1,8-diazabicyclo[5.4.0]undec-7-ene; EMTI: 4-ethyl-1-methyl-4H-[1,2,4]triazol-1-ium iodide; NBS: *N*-bromosuccinimide; DDQ: 2,3-Dichloro-5,6-dicyano-1,4-benzoquinone.

10.1002/ange.202004789

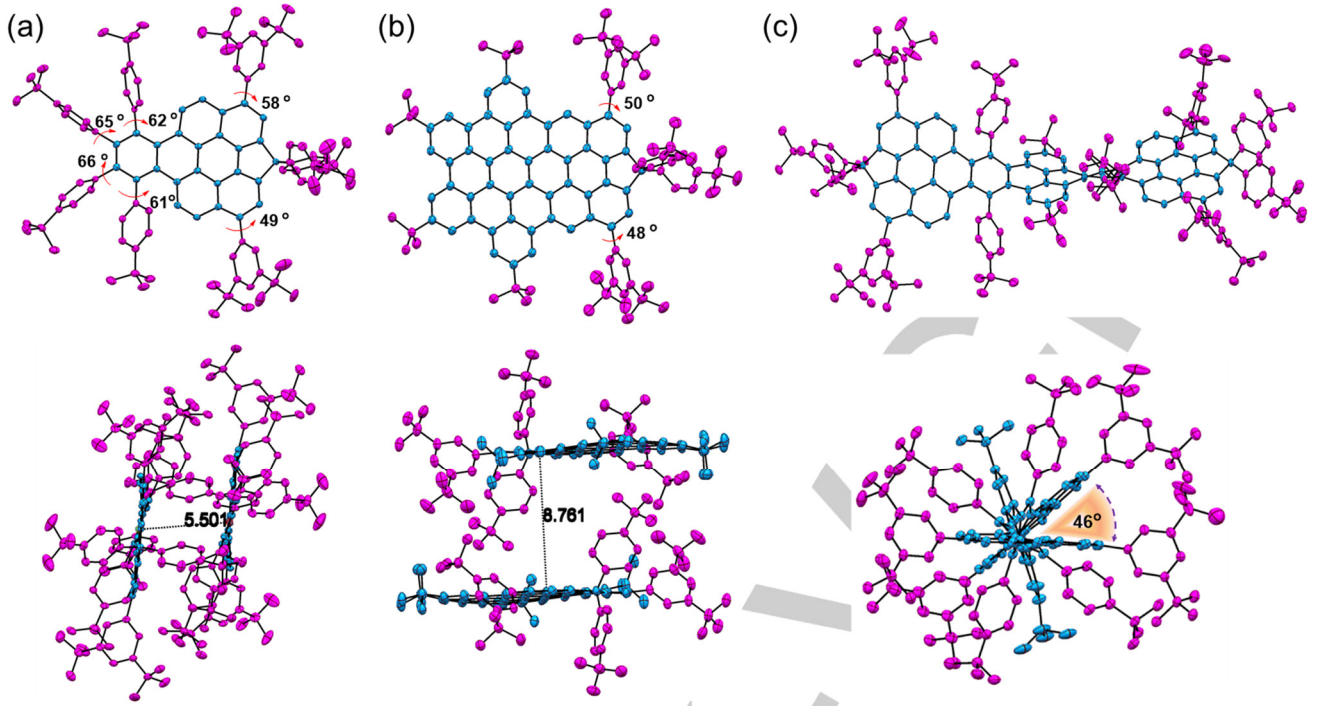

Figure 2. X-ray crystallographic structures of (a) **ZY-01**, (b) **ZY-02**, and (c) **ZY-03**, in top-view (top panels) and side-view (bottom panels). Solvent and hydrogen atoms are omitted for clarity. The π-π distances between the neighbouring molecules in **ZY-01** and **ZY-02** are labelled in black numbers with unit in Å. **ZY-03** shows a highly twisted backbone with a dihedral angle of about 46° between the two terminal perylene units.

dicyano-1,4-benzoquinone (DDQ) and methanesulfonic acid ($MeSO_3H$) in dichloromethane (DCM) at room temperature (RT) selectively resulted in the partially fused compounds **ZY-01** and **ZY-03** in 85% and 78% isolated yield, respectively. Prolongation of the reaction time did not generate the fully fused products **ZY-02** and **ZY-04**. On the other hand, Scholl reaction of **10** by using iron(III) chloride in nitromethane/DCM gave the fully fused **ZY-02** in 36% isolated yield. However, similar condition applied to the precursor **11** led to complicated mixture mainly containing partially fused products (based on mass spectrometry). In addition, treatment of **ZY-01** with iron(III) chloride successfully afforded the fully fused product **ZY-02** in 50% isolated yield, indicating that the partially fused product **ZY-01** could be a possible intermediate for the formation of **ZY-02**. On the other hand, attempted Scholl reaction from **ZY-03** by using stronger reaction conditions such as DDQ/CF_3SO_3H or $FeCl_3$ did not give fully cyclized product **ZY-04**.

X-ray crystallographic analysis. Single crystals suitable for X-ray diffraction analysis of **ZY-01**, **ZY-02** and **ZY-03** were grown by slow diffusion of methanol vapor into the toluene solution of each compound.[17] **ZY-01** has a slightly bent naphthoperylene backbone due to steric repulsion between the tetraphenylbenzene moiety and the perylene unit (torsional angle: ~ 8.6°/19.5°) (Figure 2a). All the phenyl substituents on the core are twisted significantly (torsional angle: 49° ~ 66°) and the two 4-*tert*-butylphenyl groups on the CP-ring point to the opposite sides of the perylene plane. Importantly, the distance between the backbones of neighboring molecules (about 5.501 Å) is significantly larger than typical distances for π-π interaction (~ 3.35 Å), and thus these chromophores are fully segregated in crystal. **ZY-02** displays a nearly planar, fully-fused backbone, and the slight deviation from planarity should be due to the strain induced by the five-membered CP-ring (Figure 2b). All the aryl substituents are twisted from the plane and there are even longer inter-chromophore distance (about 8.761 Å). X-ray structure of **ZY-03** clearly shows that only two C-C bonds are formed during the Scholl reaction, and the conjugated backbone exhibits a highly twisted, helical geometry (Figure 2c). Noticeably, the central eight linearly fused benzenoid rings twists about 134° from one terminal to the other one (with a dihedral angle of 46°), which is rare among the reported highly twisted helical PAHs.[18] The twisting also prevents from close π-π interaction in **ZY-03**. The right-handed and left-handed enantiomers are paired in crystals but attempted resolution by chiral HPLC was not successful.

Optical and electrochemical properties in solution. Compounds **ZY-01**, **ZY-02** and **ZY-03** are very stable and show good solubility in common organic solvents. Their UV-vis absorption and fluorescence spectra in DCM recorded at RT are shown in Figure 3. **ZY-01** shows a well-resolved absorption band with maximum (λ_{max}) at 463 nm (Figure 3a). The band structure is very similar to that of the CP-Per monomer (λ_{max} = 428 nm),[10] indicating that it still resembles the electronic properties of perylene. Time-dependent density functional theory (TD DFT) calculations suggest that this band is originated from the HOMO→LUMO electronic transition (oscillator strength f = 0.5430) (see Supporting Information (SI)). The calculated HOMO and LUMO profiles are similar to that of perylene,[11b] with little spatial distribution to the benzenoid ring at the bay region (Figure S6 in SI). There is another intense band at λ_{max} = 343 nm, which is mainly originated from HOMO-1→LUMO, HOMO→LUMO+1, and HOMO-3→LUMO electronic transitions according to TD DFT calculations (see SI). **ZY-02** displays a similar spectrum, but with λ_{max} significantly red-shifted to 426 and 553 nm, respectively, due to extended conjugation in the planar fully fused backbone (Figure 3b). **ZY-02** can be also seen as an extended HBC molecule with two zigzag edges. Similarly, the lowest energy absorption band with λ_{max} at 553 nm is originated from HOMO→LUMO electronic

10.1002/ange.202004789

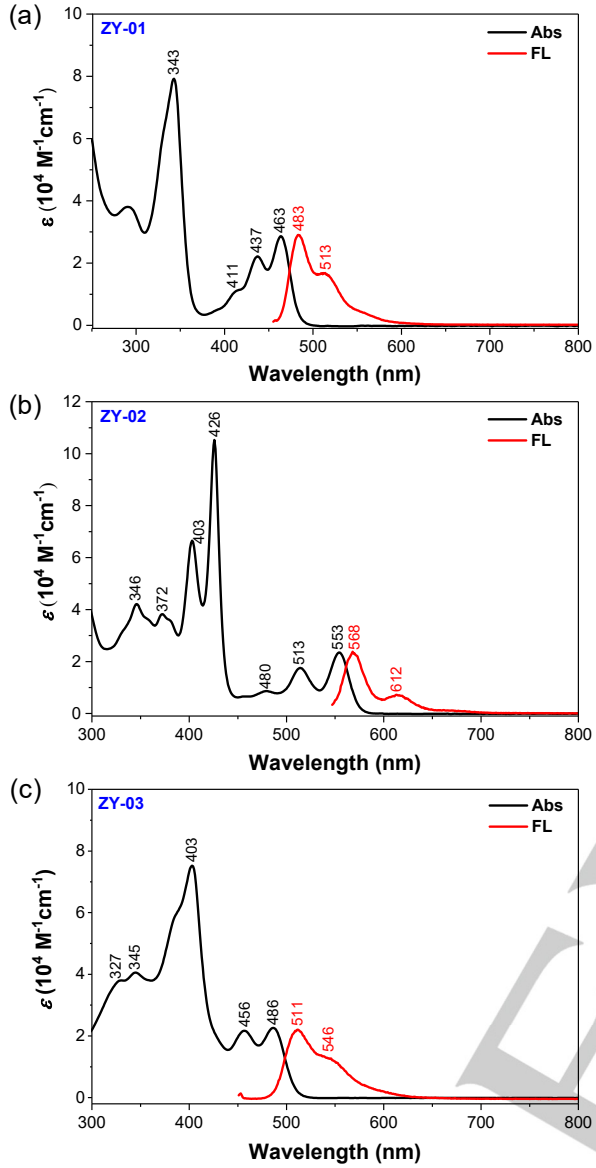

Figure 3. UV-vis absorption (Abs) and fluorescence (FL) spectra of (a) **ZY-01**, (b) **ZY-02**, and (c) **ZY-03** in DCM measured at room temperature. The excitation wavelength for the FL measurements was 455, 547 and 451 nm, respectively.

transition (f = 0.3894), and both the HOMO and LUMO are mainly distributed on the perylene units, with partial delocalization onto the HBC moiety (Figure S6 in SI). Compared to HBC derivatives, which usually exhibit forbidden low-energy electronic transitions due to its high D_{6h} symmetry,[3] the **ZY-02** with a D_{2h} symmetry demonstrates enhanced oscillator strength and molar absorptivity for the HOMO→LUMO associated excitation due to the perylene-like characteristics. The other band at λ_{max} = 426 nm can be assigned to multiple HOMO-n→LUMO+m (n = 1, 2; m = 0, 1) mono-electronic transitions, involving molecular orbitals distributed among the whole π-conjugated skeleton (see SI). **ZY-02** relative to **ZY-01** decreases the molar absorptivity (and f) due to the resemblance with HBC and thus is a perylene/HBC hybrid. The optical properties of **ZY-03** are dictated by its twited shape which makes the two respective bands overlapped with each other (Figure 3c). Hence: i) The calculated HOMO and LUMO profiles are still mainly distributed on the two terminal perylene units with small diffusion onto the central dibenzopyrene moieties (Figure S6 in SI); ii) Weak interaction between the two terminal perylene units is advised and the HOMO/HOMO-1 and LUMO/LUMO+1 are nearly degenerate (see SI); iii) the TD DFT description of the low energy excitations largely differ from that **ZY-02** with the low energy band (λ_{max} = 456/486) being originated from HOMO-n→LUMO+m (n = 0, 1; m = 0, 1) electronic transitions and the higher energy one (λ_{max} = 403 nm) owing to HOMO-2→LUMO+1 and HOMO→LUMO+2 electronic transitions (see SI).

Compounds **ZY-01**, **ZY-02** and **ZY-03** in DCM at RT all exhibit a well-resolved fluorescence spectrum with emission maximum (λ_{em}) at 483, 568 and 511 nm (Figure 3) and a moderate PLQY of 56%, 45% and 32%, respectively. The PLQY values are lower than that of perylene (which is nearly 100%), but much larger than that of HBC derivatives (usually < 3%). Furthermore, the PLQYs change according to: i) from **ZY-01** to **ZY-02** due to the HBC character of the latter and also due to the red-shift (energy gap law), and ii) from **ZY-02** to **ZY-03** due to the twisting which is known to promote non-radiative decays such as enhanced intersystem crossing (ISC).[19] Their absorption and emission spectra in 2-methyl tetrahydrofuran (2-MeTHF) (Figure S1 in SI) measured at 80 K are similar to those measured at RT (with only slight sharpening of peaks), indicating that there is little aggregation even in frozen solution state.

Cyclic voltammetry measurements revealed that all these three compounds exhibited two reversible oxidation waves with the half-wave potential $E_{1/2}^{ox}$ at 0.27/0.82 V for **ZY-01**, 0.28/0.83 V for **ZY-02**, and 0.26/0.78 V for **ZY-03** (*vs* Fc^+/Fc couple) (Figure S2 in SI). **ZY-01** exhibited two overlapped reduction waves with half-wave potential $E_{1/2}^{red}$ at -1.93 and -2.03 V, while **ZY-02** and **ZY-03** both displayed one irreversible reduction with $E_{1/2}^{red}$ at -1.52 and -2.38 V, respectively. The HOMO/LUMO energy levels were estimated to be -4.88/-2.97, -4.88/-3.55 and -4.87/-2.54 eV for **ZY-01**, **ZY-02** and **ZY-03**, respectively, from the onset of the first oxidation/reduction waves. Accordingly, the respective electrochemical energy gap was estimated to 2.01, 1.43 and 2.43 eV. The trend is in agreement with the variation of the optical gaps and of the calculated HOMO/LUMO values (Figure S6 in SI). Particularly, they have similar HOMO energy level because the HOMO is mainly localize on the perylene unit. Compared with the partially fused **ZY-01** and **ZY-03**, the fully fused **ZY-02** shows lower lying LUMO and smaller energy gap.

Optical and ASE properties in PS thin film. Thin films of the **ZY-01**, **ZY-02** and **ZY-03** dispersed in PS matrix (0.5~6 wt%) were prepared by spin-coating over transparent fused silica substrates. The film thickness h was adjusted to ensure that the waveguides support only fundamental transversal modes, propagating with a high confinement factor ($\Gamma \approx 90\%$). Such election is convenient to minimize losses, and thus to optimize the ASE performance.[20] The absorption and PL spectra of the prepared films measured at RT are shown in Figure 6 and the relevant parameters reporting the film optical properties are collected in Table 1. The spectra are very similar to those measured in solution, with shifts < 5 nm. The PLQYs were increased regarding the solution state amounting to 84% for **ZY-01** (1 wt%), 77% for **ZY-02** (0.5 wt%), and 52% for **ZY-03** (3 wt%), presumably due to the restricted rotation of the aryl substituents in rigid polymer matrix, which minimizes non-radiative decay of the excited state. These moderate-to-high PLQY values indicate good potential of these molecules for solid-state luminescence.

10.1002/ange.202004789

RESEARCH ARTICLE

Table 1. Optical and ASE properties of PS films doped with **ZY-01**, **ZY-02** and **ZY-03**.

Samples	wt% in PS[a]	PLQY[b] (%)	$\lambda_{ABS\text{-}max}$[c] (nm)	$\lambda_{PL\text{-}max}$[d] (nm)	h[e] (nm)	λ_p[f] (nm)	$\alpha[\lambda_p]$[g] ($\times 10^3$ cm^{-1})	$t_p[\lambda_p]$[i] (ns)	λ_{ASE}[j] (nm)	$FWHM_{ASE}$[k] (nm)	$E_{th\text{-}ASE}$[m] (μJ/cm^2)	$I_{th\text{-}ASE}$[m] (kW/cm^2)
ZY-01	0.5	-	330, 345	481, 512	480	355	0.3	5.65				
	1	84±10			490	355	0.6	5.65				
	3	83±6			500	355	1.5	5.65	516	6	6×10^3	1.1×10^3
	6	78±5			475	355	2.9	5.65	513	8	10^4	1.8×10^3
ZY-02	0.2	-	406, 430	566, 609	480	430	0.5	3.80				
	0.5	77±9			520	430	1.3	3.80	570	4	1.8×10^3	4.7×10^2
	1	63±7			490	430	2.2	3.80	570	4	7×10^2	1.8×10^2
	3	55±4			515	430		3.80				
ZY-03	0.5	46±10	390, 407	508, 540	495	415	0.6	3.69				
	1	46±8			520	415	1.1	3.69				
	3	52±6			470	415	2.9	3.69				

[a]Error ~0.1%; [b]PLQY, photoluminescence quantum yield; [c]Peak absorption wavelengths (maximum absorption peak is underlined); [d]Peak photoluminescence wavelengths (maximum photoluminescence peak is underlined); [e]Film thickness (error ~2%); [f]Pump wavelength; [g]Absorption coefficient at λ_p (error ~2%); [i]Pump pulse width at λ_p; [j]ASE wavelength (error is ± 0.5 nm); [k]ASE linewidth (error is ± 1 nm), defined as the full width at half maximum, FWHM, well above the threshold; [m]ASE threshold (error ~20%).

The ASE properties of the **ZY-01**, **ZY-02** and **ZY-03** doped PS films, deposited on fused silica substrates, were then evaluated by optical pumping with a pulsed laser source (see details in SI) at a wavelength (λ_p) close to one of the peaks of maximum absorption (see Table 1). The presence of ASE reflects on a narrowing of the PL spectrum at a given pump intensity, accompanied by a sudden increase of the peak and overall emission intensity. The observation of ASE is a signature of the existence of optical gain due to the dominant contribution of stimulated emission over the spontaneous one. ASE was detected in **ZY-01** and **ZY-02**, but not in **ZY-03** (Figure 4). Compounds **ZY-01** and **ZY-02** displayed a net narrowing of the PL spectrum with ASE peaks (λ_{ASE}) at 516 and 570 nm, respectively. The linewidth (defined as the full width at half maximum, FWHM) of the ASE emission ($FWHM_{ASE}$) is typically of a few nm (Table 1). Plots of the evolution of the emission linewidth with the pump intensity (Figure S3 in SI) are used to determine the ASE thresholds, $E_{th\text{-}ASE}$ or $I_{th\text{-}ASE}$, expressed in energy density or power density units. The $E_{th\text{-}ASE}$ ($I_{th\text{-}ASE}$) values for the various samples prepared are shown in Table 1 and correspond to the pump energy (power) density, at which the FWHM drops to half of its initial value. It is also seen, approximately at this threshold value, or slightly above, that the output intensity (I_{out}) experiences a drastic increase (Figure S3 in SI).

The physical mechanisms underlying the appearance of ASE in the investigated films deserve further analysis. The low temperature fluorescence spectra of all three compounds in 2-MeTHF show that upon excitation in any of the two major absorption bands, only one set of emission features with two main vibronic components at 479/511 nm in **ZY-01**, 568/615 nm in **ZY-02**, and 503/539 nm in **ZY-03** emerged (Figure S1 in SI). There are additional features in these spectra that deserve futher mention: i) the energy spacing between these two set of emission peaks in each compound is rather different, much larger in **ZY-01**

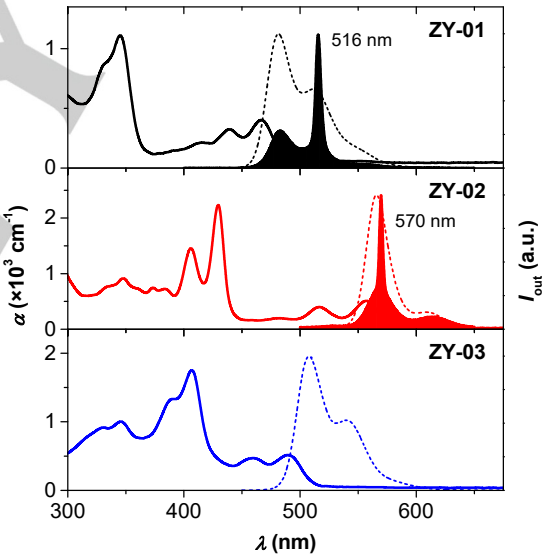

Figure 4. Optical properties at room temperature of PS films doped with 1 wt% of **ZY-01**, **ZY-02** and **ZY-03**, from top to down. Absorption coefficient, α (solid line, left axis), photoluminescence intensity (dashed line, right axis), and ASE intensity (filled area, right axis), versus wavelength, λ. PL excitation wavelength was set at the maximum of the absorption. The ASE emission for **ZY-01** is shown for PS films doped with 3 wt% of the material and no ASE emission has been observed for **ZY-03**.

(7202 cm^{-1}) and smaller in **ZY-03** (4264 cm^{-1}), with **ZY-02** at intermediate values (5463 cm^{-1}). This indicates a larger spectral congestion (smaller energy spacing) in **ZY-03**, a situation that favours non-radiative processes such as internal conversion (IC) and ISC; ii) the vibrational spacing in **ZY-02** is larger between its vibronic components of the excitation and of the emission; and iii) the Stokes shifts, conversely to point (ii), is smaller in **ZY-02**. Point (i) might become relevant in a situation of strong pumping excitation, thus pump-probe experiments with excitation in the

10.1002/ange.202004789

high energy set of bands and micro-second time detection after excitation have been carried out with their solutions in THF (Figure S4 in SI). It was found that **ZY-01** showed no transient spectra, indicating that formation of triplet excited states from the optically pumped singlet does not take place to a significant extent. However, net sets of excited state absorption (ESA) bands for triplet transient species were recorded for **ZY-02** and **ZY-03**, which are particularly strong ESA bands in **ZY-03**. This is in agreement with a greater excited state congestion of **ZY-03** upon excitation which favours ISC. In addition, the highly twisted π-conjugated backbone in **ZY-03** is a favurable condition for enhanced spin-orbit coupling futher summing to ISC.[19]

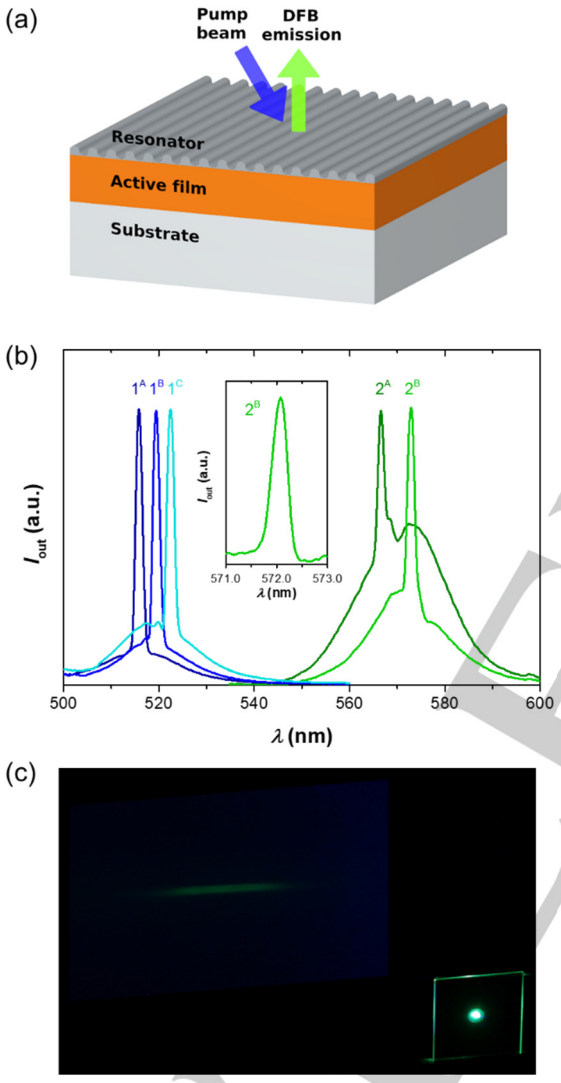

Figure 5. (a) Sketch of the DFB device, consisting of a top-layer polymeric resonator with an engraved relief grating, located over an active film of **ZY-01** or **ZY-02** dispersed in PS, deposited on a fused silica substrate. The excitation and collection geometries are shown by arrows. (b) Spectra of various DFB lasers based on **ZY-01** (blue lines) and **ZY-02** (green lines) with dye concentrations in PS of 3 wt% and 1 wt%, respectively. The number on the device label (1 or 2) refers to the compound used (**ZY-01** or **ZY-02**, respectively); the letters on the labels refer to devices with different geometrical parameters (listed in Table 2). The inset shows the the high-resolution spectrum of one of the laser peaks on an expanded scale (device 2^B). (c) Photograph of the green light emitted by laser 1^A, projected on a screen in the left top corner. The bright spot in the center of the sample is a mixture of the pump and emitted laser light.

Fabrication and characterization of DFB lasers. DFB lasers based on **ZY-01** and **ZY-02** doped PS films were fabricated. The device structure includes a top-layer polymeric resonator, consisting of a water-soluble dichromated gelatin photoresist layer with a 1D relief grating (engraved by holographic lithography), deposited on top of an active film (see scheme of the device structure in Figure 5a). The thickness of the active film (h) is constant and such device structure enables multicolour emission within a single chip while keeping a low threshold.[21] All the DFB devices prepared in this work have one-dimensional (1D) gratings and operate in the second order of diffraction. The geometrical and performance parameters of the prepared lasers are collected in Table 2. The grating period (Λ), adjusted by proper selection of grating fabrication parameters, was varied in the approximate range 328-370 nm to obtain lasing at wavelengths close to the maximum gain for each compound (that at which ASE is observed).

The prepared lasers emit at different wavelengths (λ_{DFB}) in the visible region, particularly, in the range of 515-523 nm for **ZY-01** and 566-572 nm for **ZY-02** (Figure 5b). For a given compound, λ_{DFB} was tuned by changing Λ. In all cases, single mode emission was obtained with very narrow linewidths (0.36 nm for device 2B), as seen in the high resolution spectrum shown in the inset of Figure 5b). For all the DFB lasers prepared, the emitted laser light is linearly polarized, in a direction parallel to the grating lines. This indicates that the laser mode is associated to the fundamental transverse electric waveguide mode TE_0. A photograph of the green light emitted by one of **ZY-01** lasers is shown in Figure 5c. The beam divergence observed in the direction perpendicular to the grating lines is ~ $5 \cdot 10^{-3}$ rad. The DFB thresholds of the various devices were extracted from plots of the emission linewidth (FWMH) versus E_{pump} (Figure S5 in SI). Threshold values between 400 and 680 μJ cm^{-2} (i.e., 100-175 kW cm^{-2}) have been obtained for the various devices based on **ZY-01** and somewhat larger for those based on **ZY-02.** The large values for the prepared **ZY-02** devices, can be ascribed to the fact that ASE appears at the main PL peak, instead of on the first vibronic peak (as it occurs for **ZY-01**), and consequently with large self-absorption.

Conclusion

In summary, a new strategy was developed for the synthesis of large-size aggregation-free PAHs starting from a CP-ring fused perylene building block. The existence of the CP-rings at the peripheries fully suppresses intermolecular π-π interaction, which is critical for efficient solid-state luminescence. The obtained three PAHs all display perylene-like electronic structures and optical properties with moderate-to-high PLQYs. Notably, **ZY-01** and **ZY-02**, with a nearly planar backbone, show ASE properties and solution-processed DFB lasers with tunable emission wavelengths were successfully fabricated. On the other hand, **ZY-03** with a twisted backbone did not exhibit ASE and lasing behaviour, presumably due to existence of interfering non-radiative IC and ISC processes. Our new design and synthetic strategies could be further exploited to prepare various large-size aggregation-free PAHs with controlled edge structure and tunable optical properties, and eventually for solid-state luminescence devices in the future.

Table 2. Parameters of top-layer resonator DFB lasers based on **ZY-01** and **ZY-02** as active media.

Laser device[a]	h[b] (nm)	λ_p[c] (nm)	$\alpha[\lambda_p]$[d] ($\times 10^3$ cm^{-1})	$t_p[\lambda_p]$[e] (ns)	Λ[f] (nm)	λ_{DFB}[g] (nm)	$E_{th\text{-}DFB}$[h] (μJ/cm^2)	$I_{th\text{-}DFB}$[i] (kW/cm^2)
1^A	500	439	0.87	3.86	328.7	515.8	400	100
1^B					331.6	519.4	400	100
1^C					334.2	522.4	680	175
2^A	490	430	2.2	3.80	366.4	566.7	~4×10^5	~1×10^5
2^B					370.4	572.1	~3×10^5	~8×10^4

[a]The DFB device consists of an active film of **ZY-01** or **ZY-02** dispersed in polystyrene, PS (dye contents 3 wt% and 1 wt%, respectively; error ~0.1%) with a top-layer of dichromated gelatine with an engraved relief grating. The number in the device label (1 or 2) refers to the ZY compound (**ZY-01** or **ZY-02**, respectively). The letters (A, B and C) refer to devices with different grating periods, thus emitting at different wavelengths; [b]Film thickness (error ~2%); [c]Pump wavelength; [d]Absorption coefficient at λ_p (error ~2%); [e]Pump pulse width at λ_p; [f]Grating period (error ~0.5%); [g]DFB wavelength (error is ± 0.5 nm; ± 0.1 nm for device 2^B); [h]DFB threshold (error ~20%).

Acknowledgements

J.W. acknowledges financial support from the MOE Tier 3 programme (MOE2014-T3-1-004), NRF Investigatorship (NRF-NRFI05-2019-0005), and MOE Tier 2 grant (MOE2018-T2-2-094). J.C. acknowledges Spanish Ministerio de Economía y Competitividad (MINECO) and Junta de Andalucía of Spain project references PGC2018-098533-B-I00 and UMA18FEDERJA057. The group at the University of Alicante acknowledges financial support from MINECO and the European FEDER funds through Grant MAT2015-66586-R.

Keywords: polycyclic aromatic hydrocarbon • perylene • dye • amplified spontaneous emssion • organic laser

[1] (a) J. Wu, W. Pisula, K. Müllen, *Chem. Rev.* **2007**, *107*, 718. (b) A. Narita, X. Y. Wang, X. Feng, K. Müllen, *Chem. Soc. Rev.* **2015**, *44*, 6616. (c) Y. Segawa, H. Ito, K. Itami, *Nat. Rev. Mater.* **2016**, *1*, 15002.

[2] (a) M. Kastler, W. Pisula, D. Wasserfallen, T. Pakula, K. Müllen, *J. Am. Chem. Soc.* **2005**, *127*, 4286. (b) X. Yan, X. Cui, L. Li, *J. Am. Chem. Soc.* **2010**, *132*, 5944. (c) X. Yan, X. Cui, B. Li, L. Li, *Nano Lett.* **2010,** *10*, 1869.

[3] (a) R. Becker, *Theory and Interpretation of Fluorescence and Phosphorescence*; WileyInterscience: New York, 1969. (b) M. Zander, *Fluorimetrie*; Springer-Verlag: Berlin, **1981**. (c) J. C. Fetzer, *Large (C>)24) Polycyclic Aromatic Hydrocarbons*; John Wiley & Sons: New York, **2000**. (d) C. Y. Liu, A. J. Bard, *Chem. Mater.* **2000**, *12*, 2353.

[4] (a) Z. Wang, Ž. Tomovic, M. Kastler, R. Pretsch, F. Negri, V. Enkelmann, K. Müllen, *J. Am. Chem. Soc.* **2004**, *126*, 7794. (b) M. Kastler, J. Schmidt, W. Pisula, D. Sebastiani, K. Müllen, *J. Am. Chem. Soc.* **2006**, *128*, 9526. (c) X. Feng, W. Pisula, K. Müllen, *J. Am. Chem. Soc.* **2007**, *129*, 14116. (d) T. Dumslaff, B. Yang, A. Maghsoumi, G. Velpula, K. S. Mali, C. Castiglioni, S. De Feyter, M. Tommasini, A. Narita, X. Feng, K. Müllen, *J. Am. Chem. Soc.* **2016**, *138*, 4726. (e) Q. Chen, S. Thoms, S. Stöttinger, D. Schollmeyer, K. Müllen, A. Narita, T. Basche, *J. Am. Chem. Soc.* **2019**, *141*, 16439.

[5] (a) I. D. W. Samuel, G. A. Turnbull, *Chem. Rev.* **2007**, *107*, 1272. (b) J. Clark, G. Lanzani, *Nat. Photon.* **2010**, *4*, 438. (c) S. Chénais, S. Forget, *Polym. Int.* **2012**, *61*, 390. (d) C. Grivas, M. Pollnau, *Laser Photon. Rev.* **2012**, *6*, 419. (e) A. J. C. Kuehne, M. C. Gather, *Chem. Rev.* **2016**, *116*, 12823. (f) M. Anni, S. Lattante, *Organic Lasers: Fundamentals, Developements, and Applications*; Pan Stanford Publishing, Singapore, **2018**.

[6] (a) C. Karnutsch, C. Gýrtner, V. Haug, U. Lemmer, *Appl. Phys. Lett.* **2006**, *89*, 201108. (b) C. Karnutsch, *Appl. Phys. Lett.* **2007**, *90*, 131104. (c) B. K. Yap, R. Xia, M. Campoy-Quiles, P. N. Stavrinou, D. D. C. Bradley, *Nat. Mater.* **2008**, *7*, 376. (d) R. Xia, W.-L. Lai, P. A. Levermore, W. Huang, D. D. C. Bradley, *Adv. Funct. Mater.* **2009**, *19*, 2844. (e) G. Tsiminis, Y. Wang, A. L. Kanibolotsky, A. R. Inigo, P. J. Skabara, I. D. W. Samuel, G. A. Turnbull, *Adv. Mater.* **2013**, *25*, 2826.

[7] (a) Y. Yang, R. Goto, S. Omi, K. Yamashita, H. Watanabe, M. Miyazaki, Y. Oki, *Opt. Express* **2010**, *18*, 22080. (b) V. Navarro-Fuster, E. M. Calzado, P. G. Boj, J. A. Quintana, J. M. Villalvilla, M. A. Díaz-García, V. Trabadelo, A. Juarros, A. Retolaza, S. Merino, *Appl. Phys. Lett.* **2010**, *97*, 171104. (c) M. G. Ramírez, S. Pla, P. G. Boj, J. M. Villalvilla, J. A. Quintana, M. A. Díaz-García, F. Fernández-Lázaro, Á. Sastre-Santos, *Adv. Opt. Mater.* **2013**, *1*, 933. (d) M. G. Ramírez, M. Morales-Vidal, V. Navarro-Fuster, P. G. Boj, J. A. Quintana, J. M. Villalvilla, A. Retolaza, S. Merino, M. A. Díaz-García, *J. Mater. Chem. C* **2013**, *1*, 1182. (e) M. G. Ramirez, P. G. Boj, V. Navarro Fuster, I. Vragovic, J. M. Villalvilla, I. Alonso, V. Trabadelo, S. Merino, M. A. Díaz-García, *Opt. Express* **2011**, *19*, 22443.

[8] (a) G. M. Paternm, Q. Chen, X. Wang, J. Liu, S. G. Motti, A. Petrozza, X. Feng, G. Lanzani, K. Müllen, A. Narita, F. Scotognella, *Angew. Chem. Int. Ed.* **2017**, *56*, 6753. (b) G. M. Paternò, L. Moretti, A. J. Barker, Q. Chen, K. Müllen, A. Narita, G. Cerullo, F. Scotognella, G. Lanzani, *Adv. Funct. Mater.* **2019**, *29*, 1805249.

[9] (a) Y. Gu, X. Wu, T. Y. Gopalakrishna, H. Phan, J. Wu, *Angew. Chem. Int. Ed.* **2018**, *57*, 6541. (b) V. Bonal, R. Muñoz-Mármol, F. G. Gámez, M. Morales-Vidal, J. M. Villalvilla, P. G. Boj, J. A. Quintana, Y. Gu, J. Wu, J. Casado, M. A. Díaz-García. *Nat. Commun.* **2019**, *10*, 3327.

[10] W. Zeng, Q. Qi, J. Wu, *Sci. Bull.* **2015**, *60*, 1266.

[11] (a) W. Zeng, H. Phan, T. S. Herng, T. Y. Gopalakrishna, N. Aratani, Z. Zeng, H. Yamada, J. Ding, J. Wu, *Chem* **2017**, *2,* 81. (b) W. Zeng, Q. Qi, J. Wu, *Eur. J. Org. Chem.* **2018**, 7. (c) W. Zeng, Y. Hong, S. Medina Rivero, J. Kim, J. L. Zafra, H. Phan, T. Y. Gopalakrishna, T. S. Herng, J. Ding, J. Casado, D. Kim, J. Wu, *Chem. Eur. J.* **2018**, *24*, 4944. (d) P. M. Burrezo, W. Zeng, M. Moos, M. Holzapfel, S. Canola, F. Negri, C. Rovira, J. Veciana, H. Phan, J. Wu, C. Lambert, J. Casado, *Angew. Chem. Int. Ed.* **2019**, *58*, 14467.

[12] Y. Zou, W. Zeng, T. Y. Gopalakrishna, Y. Han, Q. Jiang, J. Wu, *J. Am. Chem. Soc.* **2019**, *141*, 7266.

[13] E. G. Delany, C. L. Fagan, S. Gundala, A. Mari, T. Broja, K. Zeitler, S. J. Connon, *Chem. Commun.* **2013**, *49*, 6510.

[14] G. J. Roth, B. Liepold, S. G. Müller, H. J. Bestmann, *Synthesis* **2004**, 59.

[15] D. Lungerich, J. F. Hitzenberger, M. Marcia, F. Hampel, T. Drewello, N. Jux, *Angew. Chem. Int. Ed.* **2014**, *53*, 12231.

[16] D. Wasserfallen, M. Kastler, W. Pisula, W. A. Hofer, Y. Fogel, Z. Wang, K. Müllen, *J. Am. Chem. Soc.* **2006**, *128*, 1334.

[17] Crystallographic data with CCDC number 1992346 (**ZY-01**), 1992348 (**ZY-02**), and 1992347 (**ZY-03**) are deposited in the Cambridge Crystallographic Data Centre.

[18] (a) R. A. Pascal, Jr., *Chem. Rev.* **2006**, *106*, 480. (b) T. Fujikawa, Y. Segawa, K. Itami, *J. Am. Chem. Soc.* **2015**, *137*, 7763. (c) M. Rickhaus, M. Mayor, M. Juríček, *Chem. Soc. Rev.* **2016**, *45*, 1542. (d) W. Fan, T.

10.1002/ange.202004789

Winands, N. L. Doltsinis, Y. Li, Z. Wang, *Angew. Chem. Int. Ed.* **2017**, *56*, 15373. (e) T. Hosokawa, Y. Takahashi, T. Matsushima, S. Watanabe, S. Kikkawa, I. Azumaya, A. Tsurusaki, K. Kamikawa, *J. Am. Chem. Soc.* **2017**, *139*, 18512. (f) K. Kato, Y. Segawa, L. T. Scott, K. Itami, *Angew. Chem. Int. Ed.* **2018**, *57*, 1337. (g) Y. Zhu, Z. Xia, Z. Cai, Z. Yuan, N. Jiang, T. Li, Y. Wang, X. Guo, Z. Li, S. Ma, D. Zhong, Y. Li, J. Wang, *J. Am. Chem. Soc.* **2018**, *140*, 4222. (h) C. M. Cruz, S. Castro-Fernández, E. Maçôas, J. M. Cuerva, A. G. Campaña, *Angew. Chem. Int. Ed.* **2018**, *57*, 14782. (i) P. J. Evans, J. Ouyang, L. Favereau, J. Crassous, I. Fernández, J. Perles, N. Martín, *Angew. Chem. Int. Ed.* **2018**, *57*, 6774. (j) P. J. Evans, J. Ouyang, L. Favereau, J. Crassous, I. Fernández, J. Perles, N. Martín, *Angew. Chem. Int. Ed.* **2018**, *57*, 6774. (k) J. M. Fernández-García, P. J. Evans, S. M. Rivero, I. Fernández, D. García-Fresnadillo, J. Perles, J. Casado, N. Martín, *J. Am. Chem. Soc.* **2018**, *140*, 17188. (l) J. M. Fernánde-García, P. J. Evans, S. Filippone, M. Á. Herranz, N. Martín, *Acc. Chem. Res.* **2019**, *52*, 1565. (m) Y. Wang, Z. Yin, Y. Zhu, J. Gu, Y. Li, J. Wang, *Angew. Chem. Int. Ed.* **2019**, *58*, 587. (n) Y. Zhu, X. Guo, Y. Li, J. Wang, *J. Am. Chem. Soc.* **2019**, *141*, 5511.

[19] K. N. A. R. Mallia, V. S. Reddy, M. Hariharan, *J. Phys. Chem. C* **2016**, *120*, 8443.

[20] (a) E. M. Calzado, M. G. Ramírez, P. G. Boj, M. A. D. García, *Appl. Opt.* **2012**, *51*, 3287. (b) M. Anni, A. Perulli, G. Monti, *J. Appl. Phys.* **2012**, *111*, 093109.

[21] J. A. Quintana, J. M. Villalvilla, M. Morales-Vidal, P. G. Boj, X. Zhu, N. Ruangsupapichat, H. Tsuji, E. Nakamura, M. A. Díaz-García, *Adv. Opt. Mater.* **2017**, *5*, 1700238.

10.1002/ange.202004789

WILEY-VCH

RESEARCH ARTICLE

Entry for the Table of Contents

RESEARCH ARTICLE

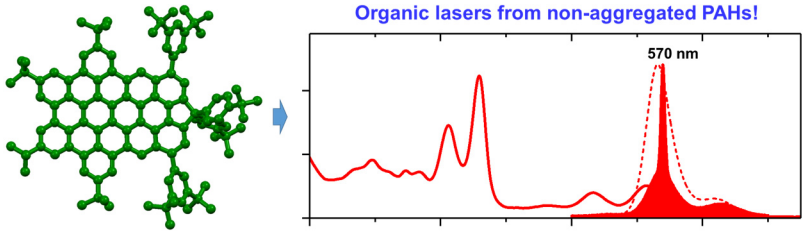

Large-size aggregation-free polycyclic aromatic hydrocarbons (PAHs) for lasers! We developed efficient synthesis of several perylene-based, aggregation-free PAHs. They show perylene-like electronic properties with moderate fluorescence quantum yields. Two of them show amplified spontaneous emission, and solution-processed distributed feedback lasers were successfully fabricated.

Y. Zou, V. Bonal, S. Moles Quintero, P.G. Boj, J.M. Villalvilla, J.A. Quintana, G. Li, S. Wu, Q. Jiang, Y. Ni, J. Casado, M.A. Díaz-García,* J. Wu**

Page xx. – Page xx

Perylene-fused, Aggregation-free Polycyclic Aromatic Hydrocarbons for Solution-processed Distributed Feedback Lasers